Table 5. iETG H I content.

KIG	HI flux [Jy km s^{-1}]	S/N	W_{50} [km s^{-1}]	log $M_{\rm HI}$ [$M_\odot$]	log $M_{\rm HI-pred}$ [$M_\odot$]
264	1.29 ± 0.10	7.6	440 ± 10	9.50	9.54
481	2.29 ± 0.25	8.8	278 ± 39	8.42	8.98

Notes. The galaxy ID is listed in Col. 1. The measured H I flux and the signal-to-noise ratio (S/N) are provided in Cols. 2 and 3. Column 4 provides W50, the velocity width at the 50% level. Columns 5 and 6 list the measured H I mass and the mass predicted by relation 17 in Jones et al. (2018) using the B-band luminosity, respectively.

sample of isolated galaxies. Only two galaxies in our sample were detected in H I (CIG 264 and 481): KIG 685, and KIG 841. They lack H I data. The others have just 5σ upper limits. Based on the distances given in Table 1, Table 5 reports the measured H I masses (Col. 5) and the expected H I mass (Col. 6) according to the relations provided in Jones et al. (2018). With the iETG upper limits, the log $M_{\rm HI-pred}$ provides values in the range of KIG 264 and KIG 418, that is, similar to median values for spirals (log $M_{\rm HI}/M_\odot = 9.47$, 9.84, and 9.59 for $T \leq$, $3 < T < 5$, and $T \geq 5$, respectively). We are aware that the relations in Jones et al. (2018) were derived from a sample that is dominated by spirals because they are the vast majority of the AMIGA galaxies.

In the HI survey of ATLAS^{3D} ETGs, Serra et al. (2012) observed KIG 637 (NGC 5687). They reported an upper limit that after adjustment to our distance (Table 1) and homogeneisation to Jones et al. (2018) is log $M_{\rm HI}\langle 8.12\ M_\odot$. Serra et al. (2012) only detected about 40% of field ETGs, therefore this tight limit by itself does not suggest that other iETG are necessarily poor in H I.

We conclude that (1) for most of these iETGs, an H I component cannot be excluded because the expected HI content is generally below the upper limits of the surveys, and (2) the two existing detections in shell galaxies are in the range of the H I-rich ETGs in the Serra et al. (2012) data set.

5.3. iETGs in the (NUV-r) versus M_r colour magnitude diagram

Colour magnitude diagrams (CMDs hereafter), in particular those built in UV versus optical bands, have been shown to be a powerful tool for understanding the evolutionary phases of galaxies. In the plane M_r versus (NUV-r), galaxies occupy well-defined positions (see e.g. Wyder et al. 2007). Evolved galaxies, ETGs, and star-forming late-type galaxies are located in two well-populated and separated areas of the CMD called the red sequence and the blue cloud, respectively. The intermediate area, less populated by galaxies, has been labelled green valley (Kaviraj et al. 2007; Schawinski et al. 2007). This area is believed to be populated by transforming galaxies. Mazzei et al. (2019) showed the evolutionary path followed by galaxies when either encounter or mergers drive their evolution. Starting their evolution in the blue cloud as disc galaxies, they reach a point of maximum brightness before they start to quench their star formation and cross the green valley. They finally reach the red sequence and in the meantime modify their morphology and kinematic properties to become mature ETGs. The crossing time of the green valley depends on their mass (brightness). It lasts >4 Gyr for the faintest ETGs.

Figure 10 shows the M_r versus (NUV-r) CMD of our targets. The dotted vertical lines, as derived from Fig. 8 in Mazzei et al. (2019), show the crossing time of the green valley as a function of the intrinsic brightest magnitude reached by simulated ETGs during their evolution in the blue cloud (see the quoted paper for a quantitative definition of different regions of the UV CMD and the evolutionary paths of the galaxies). All our iETGs have left the blue cloud. Some of them, both with and without a shell (red squares and orange dots, respectively), are still found in the green valley, but they mainly populate the red sequence.

The Mazzei et al. (2019) smoothed particle hydrodynamics simulations with chemo-photometric implementation, anchored to global properties of 11+8 ETGs, showed that the luminosities of these ETGs fade away by 0.5 mag on average, after they reached the brightest point in the blue cloud, and the galaxies enter in the green valley. On this basis, the four iETGs in the green valley will spend between 1 up to 3 Gyr in this area before they reach the red sequence. iETGs that are located in the red sequence on average took less than 3 Gyr to reach it. However, it is unknown how long they have been and will remain in the red sequence. A careful analysis and a match of their global multi-wavelength properties are required to constrain our smoothed particle hydrodynamics simulations with chemo-photometric implementation, to understand their formation mechanisms and their evolutionary path (Mazzei et al. 2014b, 2019). This will be the subject of a forthcoming paper.

We investigated if iETGs in the red sequence are so-called red-and-dead systems. It is known that the star formation in ETGs in the red sequence cannot be entirely quenched because *secondary* episodes of star formation can still be revealed. Their signatures have been found from optical to UV and mid-IR wavelengths (see e.g. Annibali et al. 2007; Rampazzo et al. 2007, 2013; Panuzzo et al. 2007, 2011; Jeong et al. 2009; Salim & Rich 2010; Thilker et al. 2010; Marino et al. 2011a,b; Cattapan et al. 2019, and references therein). The Mazzei et al. (2019) simulations suggest that these phenomena are activated during the post-merging evolution of iETGs. In this context, KIG 264, a former AGN, has already reached the red sequence, where most of our iETGs are located, and it still shows the remains of this activity.

6. Summary and conclusions

We presented the morphological and photometric study of 20 iETGs from the AMIGA catalogue (Verdes-Montenegro et al. 2005) that are bona fide ETGs according to the revised classification of Fernandez-Lorenzo et al. (2012). The revised classification contains about 100 ETGs. Although the morphological classification has been revised both visually (Buta et al. 2019) and quantitatively (Hernández-Toledo et al. 2008) using SDSS, several discrepancies remain. One of our task has been to test the reliability of the above morphological classifications in the light of deep imaging in a quantitative way.

The AMIGA isolation criteria have been refined by Verley et al. (2007a) and by Argudo-Fernàndez et al. (2013). Four of the iETGs considered in this paper fulfil the Verley et al. (2007a) isolation criteria with a trend to present a larger number of minor companions (higher η_k value), while 10 out of 20 are strictly isolated for Argudo-Fernàndez et al. (2013) (who lack spectroscopic information for 4 galaxies in the sample, however), the other is expected to be only minimally affected by any neighbours. The iETGs in our sample are hence isolated from major companions and located in poorly populated environments.

Galaxies were observed in the g and r SLOAN bands at the 1.8m VATT telescope with the 4KCCD. The light profiles on the average reach $\mu_g = 28.11 \pm 0.70$ mag arcsec^{-2} and $\mu_r = 27.36 \pm 0.68$ mag arcsec^{-2}, which makes this sample the

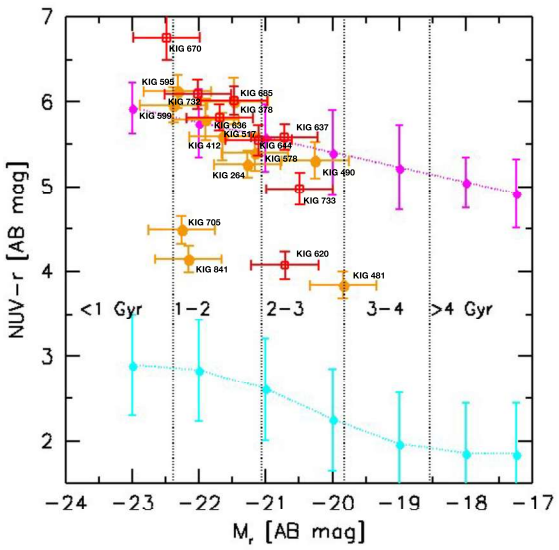

Fig. 10. UV-optical CMD of iETGs. In the M_r vs. (NUV-r) plane we plot the Wyder et al. (2007) fits to the red sequence (magenta dots and dotted line) and to the blue cloud (cyan dots and dotted line). iETGs with a shell system are indicated with orange dots. KIG 722 is missing from the iETGs sample because no NUV measures are available. The dotted vertical lines provide an indication of the green valley crossing time as a function of the galaxy luminosity (see text). The horizontal error bar accounts for a distance uncertainty of 10%. The vertical error bar accounts for the NUV ZP uncertainty, 0.15 mag (Bai et al. 2015).

deepest observations of iETGs so far. We used the AIDA package for the 2D photometric analysis and accounted for PSF effects during the decomposition of the light profiles up to the galaxy outskirts. We used the current literature to discuss thepg morphology of the residuals obtained after the 2D model subtraction from the original image. We list our results below.

- All the galaxies in the sample are bona fide ETGs, from Es to late S0s. None is a misclassified spiral.pg
- Fourteen out of 20 iETG light profiles are best fit by B+D model.pg The average B/T is 0.66 in both bands, indicating that the bulge dominates the galaxy light distribution.pg
  H-T found that bona fide Es are rare among iETGs. KIG 578, KIG 705,pg and KIG 722 are best fit by a simple Sérsic law whose exponent is near to a classic de Vaucouleurs law (see Table 4). These galaxies are in the Es set of H-T. However, we fit KIG 264, KIG 599, and KIG 732 best with a B+D model. These galaxies are all in the H-T Es bona fide sample. Our B+D models failed to provide an acceptable description of the light distribution of iETGs with type close to 0, KIG 620, KIG 644, and KIG 733 because strong additional features such as one or more rings and wide arms are present in their central region. For the latter, Buta et al. (2019) provided the best classification. Their one or more rings may be interpreted in either the framework of resonances or other phenomena that have been described as a consequence of secular evolution (see e.g. Còmeron et al. 2014; Buta et al. 2010; Laurikainen et al. 2010, 2011) or as a consequence of merging (see e.g. Eliche-Moral et al. 2018; Mazzei et al. 2019, and references therein).
- Most of our iETGs show fine structures such as shells, tails, residual faint rings, stellar fans, and a residual spiral arm-like structure after model subtraction. These features are considered signatures of accretion and merging events in the literature.
- In 12 out of 20 (60%) of the iETGs, we detected shells. They compete with rings (10 out of 20) for the most frequently dectected fine structures (see also Tal et al. 2009). This percentage is confirmed also when we considered the set of iETGs that was smaller because stricter isolation criteria were used. H-T also found very many shell galaxies in isolated ETGs. However, in Table 6 of H-T, the detection of 4 out of 9 shells and ripples was uncertain, while we revealed shells in KIG 264, KIG 578, KIG 722, and KIG 732, which are listed in that table. This is expected because H-T used more shallow images (see the considerations in Mancillas et al. 2019).
- Most (≈80%) of the iETGs are located in the red sequence in the (NUV-r) versus M_r CMD diagram. Seven out of 15 (KIG 722 lacks NUV data) show a shell structure. Four galaxies, that is, KIG481, KIG 620, KIG 705, and KIG 841, are still located in the green valley. Three of them have shells. Several other features connected to accretion and merging events are found in iETGs that are located in the red sequence.
- Fourteen iETGs have nearly flat $(g-r)$ colour profiles at ≈0.7–0.8 mag. These are normal values for early-type galaxies. We measured $(g-r)$ colour profiles that become increasingly blue with radius for KIG 481, KIG 620, and KIG 841, at least in some regions. In contrast, quite red colours are measured in the outskirts for KIG 264 and KIG 378, suggesting the presence of dust. Dust is normally expected in the galaxy centre.
  In a small number of iETGs, the blue $(g-r)$ colour profile may suggest a recent star formation episode by the high fraction of accretion and merging signatures. However, the time required to cross the (NUV-r) versus M_r plane from the green valley to the red sequence is relatively long, as shown in Fig. 10. This suggests that iETGs have had enough time to quench their star formation and AGN activity (as in KIG 264) in the case of wet mergers as well. This is in contrast to H-T and Tal et al. (2009), who suggested that dry mergers might provide a possible explanation of the evolution of these galaxies.
- The prediction by Jones et al. (2018) about the H I content of our iETGs needs to be confirmed with deep 21 cm observations because they are based on a relation fit with a sample dominated by spiral galaxies. The wide morphological disturbance in the galaxy outskirts and the measure of $M_{\rm H\,I}$ for KIG 264 and KIG 481 suggest that H I might have fuelled galaxy rejuvenation and AGN activity, as has been found in low-density environments (see e.g. Annibali et al. 2007, 2010).

The subsample of iETGs we studied presents a different behaviour from isolated late-type galaxies from the same AMIGA sample, showing a significantly higher number of perturbation signatures. Consistently, Fernandez-Lorenzo et al. (2013) found no difference in the stellar mass size relation between iETGs and counterparts in more dense environments, unlike late-type galaxies. We conclude that a significant fraction of our iETGs are a by-product of a merger. The high fraction of shells, a long-lasting fine structure in isolated and poorly populated environments, indicates that iETGs have not been perturbed for a long time (up to 3 Gyr). This is consistent with their degree of isolation. The crossing time required to move galaxies from the green valley to the red sequence in the M_r versus (NUV-r) CMD is consistent with this view. Shell galaxies that are found in the green valley will accumulate in the red sequence. Because of their isolation, iETGs appear as the cleanest environment for investigating a wide phenomenology (structure and sub-structure formation, duration, evolution, AGN feeding and fading, and star formation ignition and quenching) induced by both accretion and merging episodes.

Acknowledgements. A. O. and R. R. are deeply grateful to Fathers Richard Boyle SJ, Paul Gabor SJ and Jean-Baptiste Kikwaya SJ for assistance at the telescope. RR thanks the Specola Vaticana Director Brother Guy Consolmagno, Father Christopher Corbally and Father Thomas Williams SJ for the kind hospitality in Tucson (AZ-USA). R.R. and P.M. acknowledge funding from the INAF PRIN-SKA 2017 program 1.05.01.88.04. MGJ is supported by a Juan de la Cierva formación fellowship (FJCI-2016-29685). MGJ and LVM also acknowledge support from the grants AYA2015-65973-C3-1-R and RTI2018-096228-B-C31 (MINECO/FEDER, UE). This work has been supported by the Spanish Science Ministry "Centro de Excelencia Severo Ochoa" program under grant SEV-2017-0709. `IRAF` is distributed by the National Optical Astronomy Observatories, which are operated by the Association of Universities for Research in Astronomy, Inc., under cooperative agreement with the National Science Foundation. This research has made use of the NASA/IPAC Extragalactic Database (NED), which is operated by the Jet Propulsion Laboratory, California Institute of Technology, under contract with the National Aeronautics and Space Administration. We acknowledge the usage of the `HyperLeda` database (`http://leda.univ-lyon1.fr`).

References

Abazajian, K. N., Adelman-McCarthy, J. K., Agüeros, M. A., et al. 2009, ApJS, 182, 543
Akhlaghi, M., & Ichikawa, T. 2015, ApJS, 220, 1
Atkinson, A. M., Abraham, R. G., & Ferguson, A. M. N. 2013, ApJ, 765, 28
Argudo-Fernàndez, M., Verley, S., Bergond, G., et al. 2013, A&A, 560, A9
Argudo-Fernàndez, M., Verley, S., Bergond, G., et al. 2015, A&A, 578, A110
Arp, H. 1966, ApJS, 14, 1
Annibali, F., Bressan, A., Rampazzo, R., Zeilinger, W. W., & Danese, L. 2007, A&A, 463, 455
Annibali, F., Bressan, A., Rampazzo, R., et al. 2010, A&A, 519, A40
Bai, Y., Zou, H., Liu, J., et al. 2015, ApJS, 220, 6
Bennert, N., Canalizo, G., Jungwiert, B., et al. 2008, Mem. Soc. Astron. It., 79, 1247
Bertin, E., Mellier, Y., Radovich, M., et al. 2002, Astron. Data Anal. Softw. Syst. XI, 281, 228
Bevington, P. R. 1994, Data Reduction and Error Analysis for the Physical Sciences (McGraw-Hill)
Buta, R. J., Seth, K., Athanassoula, E., et al. 2015, ApJS, 217, 32
Buta, R. J., Verdes-Montenegro, L., Damas-Segovia, A., et al. 2019, MNRAS, 488, 2175
Buta, R. J., Laurikainen, E., Salo, H., & Knapen, J. H. 2010, ApJ, 721, 259
Cappellari, M. 2016, ARA&A, 54, 597
Cattapan, A., Spavone, M., Iodice, E., et al. 2019, ApJ, 874, 130
Clemens, M. S., Bressan, A., Nikolic, B., et al. 2006, MNRAS, 370, 702
Clemens, M. S., Bressan, A., Nikolic, B., & Rampazzo, R. 2009, MNRAS, 392, L35
Combes, F., Rampazzo, R., Bonfanti, P. P., Pringniel, P., & Sulentic, J. W. 1995, A&A, 297, 37
Còmeron, S., Salo, H., Laurikainen, E., et al. 2014, A&A, 562, A121
Costantin, L., Corsini, E. M., Méndez-Abreu, J., et al. 2018, MNRAS, 481, 3623
Côtè, P., Piatek, S., Ferrarese, L., et al. 2006, ApJS, 165, 57
de Vaucouleurs, G. 1953, MNRAS, 113, 134
Donzelli, C. J., Muriel, H., & Madrid, J. P. 2011, ApJS, 195, 15
Dressler, A. 1980, ApJ, 236, 351–365
Duc, P.-A., Cuillandre, J.-C., Karabal, E., et al. 2015, MNRAS, 446, 120
Dupraz, C., & Combes, F. 1987, A&A, 185, 1
Erwing, P. 2015, ApJ, 799, 226
Fernandez-Lorenzo, M., Sulentic, J. W., Verdes-Montenegro, L., et al. 2012, A&A, 540, A47
Fernandez-Lorenzo, M., Sulentic, J. W., Verdes-Montenegro, , & Argudo-Fernadez, M. 2013, MNRAS, 434, 325
Freeman, K. C. 1970, ApJ, 160, 811
Giovanelli, R., Haynes, M. P., & Chincarini, G. L. 1982, ApJ, 262, 442
Genel, S., et al. 2014, MNRAS, 445, 175
Goto, T., Yamauchi, C., Fujita, Y., et al. 2003, MNRAS, 346, 601
Eliche-Moral, M., Rodriguez-Perez, C., Borlaff, A., et al. 2018, A&A, 617, A113
Gaditti, D. A. 2009, MNRAS, 393, 1531
Gonzalez, A. H., Zabludoff, A. I., & Zaritsky, D. 2005, ApJ, 618, 195
Hagen, L. M. Z., Seibert, M., Hagen, A., et al. 2016, ApJ, 826, 210
Hernàndez-Ibarra, F., Dultzin, D., Krongold, Y., et al. 2013, MNRAS, 434, 336
Hernández-Toledo, H. M., Vázquez-Mata, J. A., Martínez-Vízquez, L. A., et al. 2008, AJ, 136, 211 H-T
Hernández-Toledo, H. M., Vázquez-Mata, J. A., Martínez-Vízquez, L. A., et al. 2010, AJ, 139, 2525
Ho, L. C., Zhao-Yu, L., Barth, A. J., et al. 2011, ApJS, *197*, 21: CGS
Huang, S., Ho, L. C., Peng, C. Y., Li, Z.-Y., & Barth, A. J. 2013, ApJ, 766, 47
Houghton, R. C. W. 2015, MNRAS, 451, 3427
Infante-Sainz, R., Trujillo, I., & Román, J. 2020, MNRAS, 491, 5317
Jedrzejewski, R. I. 1987, MNRAS, 226, 747
Jeong, H., Yi, S. K., Bureau, M., et al. 2009, MNRAS, 398, 2028
Jones, M. G., Espada, D., Verdes-Montenegro, L., et al. 2018, A&A, 609, A17
Karabal, E., Duc, P.-A., & Kuntschner, H. 2017, A&A, 601, A86
Karachentseva, V. 1973, Astrof. Issledovanija Byu. Spec. Ast. Obs., 8, 3
Kaviraj, S., Schawinski, K., Devriendt, J. E., et al. 2007, ApJS, 173, 619
Lauer, T. R., Faber, S. M., Holtzman, J. A., et al. 1991, ApJ, 369, L41
Lauer, T. R., Faber, S. M., Currie, D. G., et al. 1992, AJ, 104, 552
Lauer, T. R. 2012, ApJ, 759, 64
Laurikainen, E., Salo, H., Buta, R. J., et al. 2010, MNRAS, 405, 1089
Laurikainen, E., Salo, H., Buta, R. J., et al. 2011, MNRAS, 418, 1452
Li, Z.-Y., Ho, L. C., Barth, A. J., et al. 2011, ApJS, 197, 22
Longhetti, M., Bressan, A., Chiosi, C., & Rampazzo, R. 1999, A&A, 345, 419
Malin, D. F., & Carter, D. 1983, ApJ, 274, 534
Mancillas, B., Duc, P.-A., Combes, F., et al. 2019, A&A, 632, A122
Mapelli, M., Marino, A., & Rampazzo, R. 2015, A&A, 575, A16
Marion, G.H. 2010, CBET, 2440
Markwardt, C. B. 2008, ASP Conf. Ser., 411, 251
Marino, A., Bianchi, L., Rampazzo, R., et al. 2011a, ApJ, 736, 154
Marino, A., Rampazzo, R., Bianchi, L., et al. 2011b, MNRAS, 411, 311
Martin, D. C., Fanson, J., Schiminovich, D., et al. 2006, ApJ, 619, L1
Mazzei, P., Marino, A., Rampazzo, R., et al. 2014a, Adv. Space Res., 53, 950
Mazzei, P., Marino, A., & Rampazzo, R. 2014b, ApJ, 782, 53
Mazzei, P., Marino, A., Rampazzo, R., et al. 2018, A&A, 610, A8
Mazzei, P., Rampazzo, R., Marino, A., et al. 2019, ApJ, 885, 165
Meert, A., Vikram, V., & Bernardi, M. 2015, MNRAS, 446, 3943
Moore, B., Lake, G., & Katz, N. 1998, ApJ, 495, 139
Morales, G., Martínez-Delgado, D., Grebel, E. K., et al. 2018, A&A, 614, A143
Mould, J. R., Huchra, J. P., Freedman, W. L., et al. 2000, ApJ, 529, 786
Panuzzo, P., Vega, O., Bressan, A., et al. 2007, ApJ, 656, 206
Panuzzo, P., Rampazzo, R., Bressan, A., et al. 2011, A&A, 528, A10
Peng, C. Y., Ho, L. C., Impey, C. D., & Rix, H.-W. 2010, AJ, 139, 2097
Pop, A.-R., Pillepich, A., Amorisco, N. C., & Hernquist, L. 2018, MNRAS, 480, 1785
Prieur, J.-L. 1988, ApJ, 326, 596
Rabien, S., Angel, R., Barl, L., et al. 2019, A&A, 621, A4
Rampazzo, R., Marino, A., Tantalo, R., et al. 2007, MNRAS, 381, 245
Rampazzo, R., Panuzzo, P., Vega, O., et al. 2013, MNRAS, 432, 374
Rampazzo, R., et al. 2016, Astrophys. Space Sci. Lib., 435, 381
Rampazzo, R., Mazzei, P., Marino, A., Bianchi, L., Plana, H., Trinchieri, G., Uslenghi, M., & Wolter, A. 2018, Ap&SS, 363, 80
Rampazzo, R., Uslenghi, M., Georgiev, I., et al. 2019, Astron. Nachr., 341, 10
Reduzzi, L., Longhetti, M., & Rampazzo, R. 1996, MNRAS, 282, 149
Rosario, D. J., et al. 2013, ApJ, 771, 63
Salim, S., & Rich, R. M. 2010, ApJ, 714, 290
Sandin, C. 2014, A&A, 567, A97
Sandin, C. 2015, A&A, 577, A106
Serra, P., Oosterloo, T., Morganti, R., et al. 2012, MNRAS, 422, 1835
Sérsic, J. L. 1968, Atlas de Galaxias Australes (Cordoba, Argentina: Observatorio Astronomico)
Schawinski, K., Kaviraj, S., Khochfar, S., et al. 2007, ApJS, 173, 512
Silverman, J. M., Choi, J., & Filippenko, A. V. 2010, CBET, 2443
Simard, L., Mendel, T. J., Patton, D. R., et al. 2011, ApJS, 196, 11
Slater, C. T., Harding, P., & Mihos, J. C. 2009, PASP, 121, 1267
Sulentic, J. W., Verdes-Montenegro, L., Bergond, G., et al. 2006, A&A, 449, 937
Tal, T., van Dokkum, P., Nelan, J., et al. 2009, AJ, 138, 1417
Thilker, D. A., Bianchi, L., Schiminovich, D., et al. 2010, ApJ, 714, L171
Trujillo, I., & Fliri, J. 2016, ApJ, 823, 123
Turner, M. L., Côtè, P., Ferrarese, L., et al. 2012, ApJS, 203, 5
Uslenghi, M., & Falomo, R. 2011, SPIE, 8135, 24
Verdes-Montenegro, L., Sulentic, J., Lisenfeld, U., et al. 2005, A&A, 436, 443
Verley, S., Leon, S., Verdes-Montenegro, L., et al. 2007a, A&A, 472, 121
Verley, S., Odewahn, S. C., Verdes-Montenegro, L., et al. 2007b, A&A, 470, 505
Vogelsberger, M., et al. 2014a, MNRAS, 444, 1518
Vogelsberger, M., et al. 2014b, Nature, 509, 177
York, D. G., et al. 2000, AJ, 120, 1579
Weil, M. L., & Hernquist, L. 1993, ApJ, 405, 142
Wilkinson, A., Prieur, J.-L., Lemoine, R., et al. 2000, MNRAS, 319, 977
Wong, I. O., Schawinski, K., Jòsza, G. I. G., et al. 2015, MNRAS, 447, 3311
Wyder, T. K., Martin, C. D., Schiminovic, D., et al. 2007, ApJS, 173, 293

Appendix A: iETG surface photometry

In this section we show the photometric analysis we performed on each galaxy. The figures show the g (left panel) and r (right panel) results described in detail in Sect. 4 and discussed in Sect. 5.

Each panel shows the model of the galaxy we adopted, the residual after the model subtraction, the luminosity profile in the filter, and the residual (O-C) from the model we adopted.

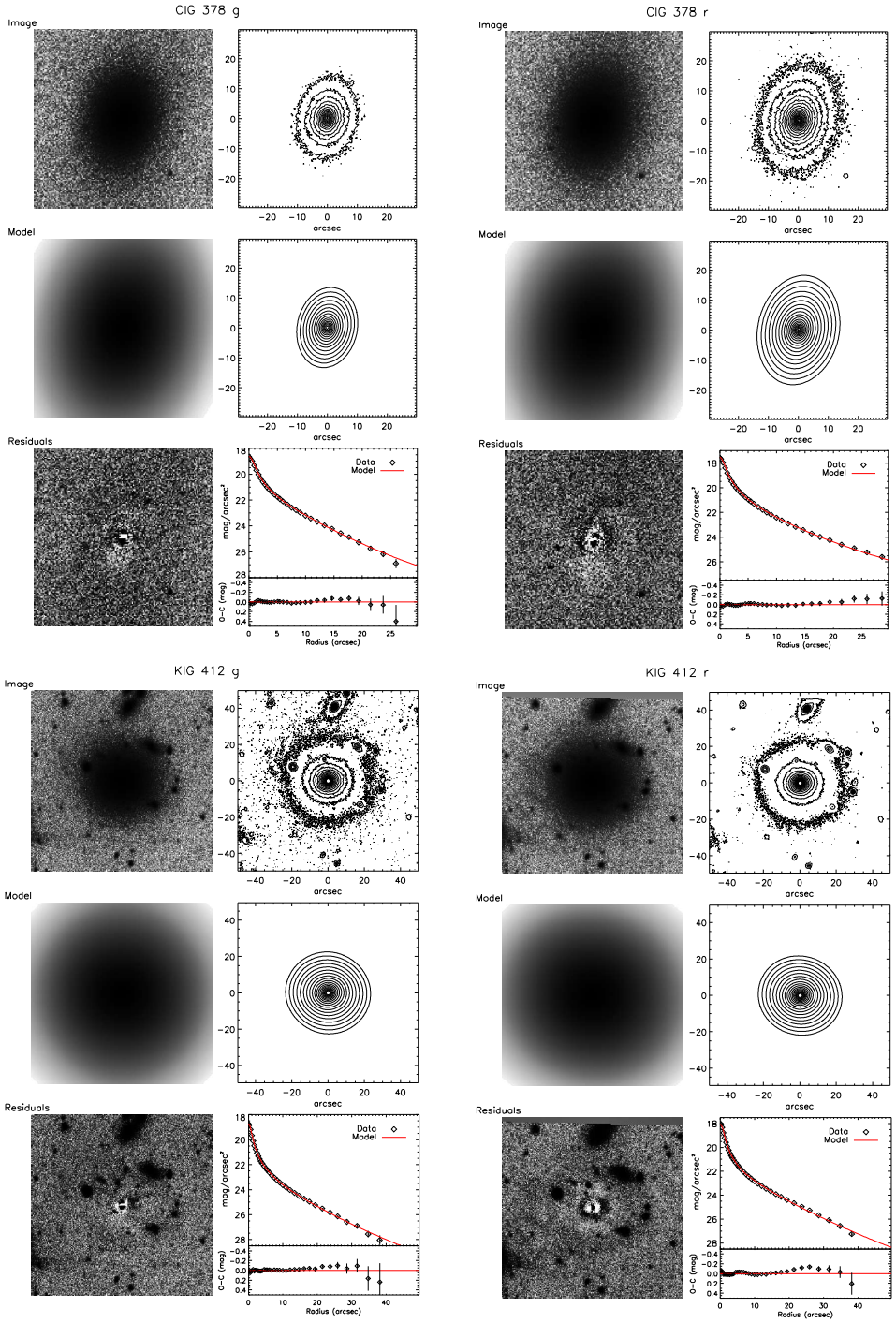

Fig. A.1. As in Fig. 5. Summary of the surface photometric analysis of KIG 378 (*top panels*) and KIG 412 (*bottom panels*). In both bands we show the B+D best-fit models. We show 20 isophote levels, between 500 and 2 σ of the sky level, for the original and model images.

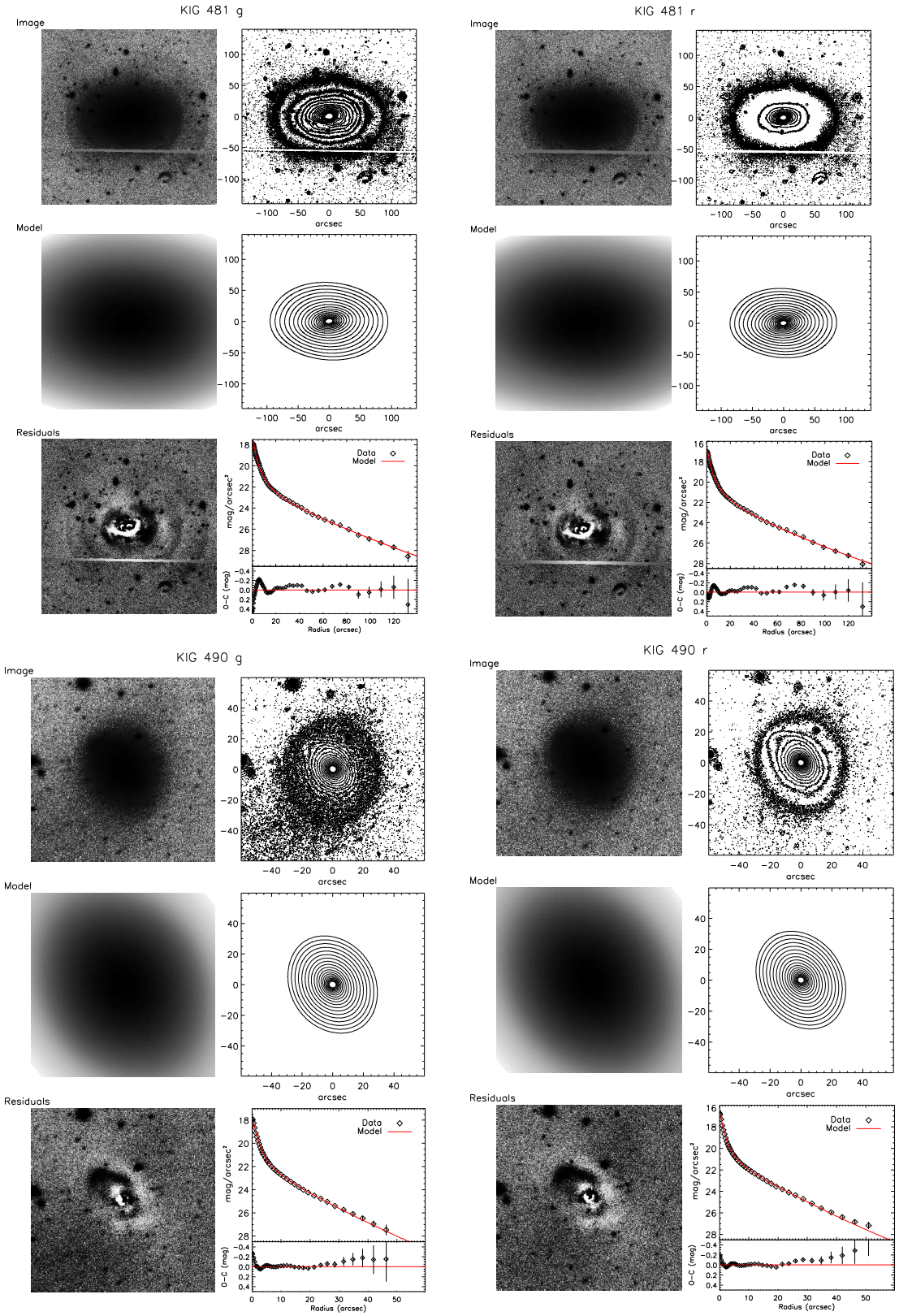

Fig. A.2. As in Fig. 5. Summary of the surface photometric analysis of KIG 481 (*top panels*) and KIG 490 (*bottom panels*). In both bands the B+D best-fit models are shown. The KIG 481 image shows the gap in the 4K CCD and a dust feature that was not removed by the flat-fielding. We show 20 isophote levels, between 500 and 2σ of the sky level, for the original and model images.